JGR Atmospheres

RESEARCH ARTICLE
10.1029/2018JD030228

Effects of Particle Nonsphericity on Dust Optical Properties in a Forecast System: Implications for Model-Observation Comparison

G. A. Hoshyaripour[1], V. Bachmann[2], J. Förstner[2], A. Steiner[2], H. Vogel[1], F. Wagner[1], C. Walter[1], and B. Vogel[1]

[1]Institute of Meteorology and Climate Research, Karlsruhe Institute of Technology (KIT), Karlsruhe, Germany, [2]Deutscher Wetterdienst (DWD), Offenbach, Germany

Key Points:
- Nonspherical dust particles increase the optical depth by up to 28%
- Model-observation agreement with respect to AOD slightly enhances by considering nonsphericity
- Accounting for nonsphericity improves the model skill with respect to attenuated backscatter

Correspondence to:
G. A. Hoshyaripour,
ali.hoshyaripour@kit.edu

Citation:
Hoshyaripour, G. A., Bachmann, V., Förstner, J., Steiner, A., Vogel, H., Wagner, F., et al. (2019). Effects of particle nonsphericity on dust optical properties in a forecast system: Implications for model-observation comparison. *Journal of Geophysical Research: Atmospheres*, *124*, 7164–7178. https://doi.org/10.1029/2018JD030228

Received 18 JUN 2018
Accepted 24 MAY 2019
Accepted article online 7 JUN 2019
Published online 2 JUL 2019

Author Contributions

Conceptualization: G. A. Hoshyaripour, J. Förstner, A. Steiner, H. Vogel, F. Wagner, B. Vogel
Data curation: G. A. Hoshyaripour, V. Bachmann, A. Steiner, F. Wagner
Funding Acquisition: H. Vogel, B. Vogel
Methodology: G. A. Hoshyaripour, J. Förstner, A. Steiner, H. Vogel, F. Wagner, C. Walter, B. Vogel
Software: G. A. Hoshyaripour, J. Förstner, A. Steiner, C. Walter
Validation: G. A. Hoshyaripour, V. Bachmann, A. Steiner, F. Wagner
Writing - Original Draft: G. A. Hoshyaripour, V. Bachmann, A. Steiner, H. Vogel, F. Wagner, B. Vogel

Abstract Mineral dust is a key player in the Earth system that affects the weather and climate through absorbing and scattering the radiation. Such effects strongly depend on the optical properties of the particles that are in turn affected by the particle shape. For simplicity, dust particles are usually assumed to be spherical. But this assumption can lead to large errors in modeling and remote sensing applications. This study investigates the impact of dust particle shape on its direct radiative effect in a next-generation atmospheric modeling system ICON-ART (ICOsahedral Nonhydrostatic weather and climate model with Aerosols and Reactive Trace gases) to verify if accounting for nonsphericity enhances the model-observation agreement. Two sets of numerical experiments are conducted by changing the optical shape of the particles: one assuming spherical particles and the other one assuming a mixture of 35 randomly oriented triaxial ellipsoids. The simulations are compared to MISR (Multiangle Imaging Spectroradiometer), AERONET (Aerosol Robotic Network), and CALIPSO (Cloud-Aerosol Lidar and Infrared Pathfinder Satellite Observation) observations (with focus on North Africa). The results show that consideration of particle nonsphericity increases the dust AOD (Aerosol Optical Depth) at 550 nm by up to 28% and leads to slight enhancement of the agreement between modeled and measured AOD. However, the model performance varies significantly when focusing on specific regions in North Africa. These differences stem from the uncertainties associated with particle size distribution and emission mechanisms in the model configuration. Regarding the attenuated backscatter, the simulated profile assuming nonsphericity differs by a factor of 2 to 5 from the experiment assuming spherical dust and is in a better agreement with the CALIPSO observations.

1. Introduction

Mineral dust is the most dominant atmospheric aerosol by mass (IPCC, 2013; Textor et al., 2006), which is emitted mainly through wind erosion of the low-vegetated land surfaces in arid and semiarid regions (Shao, 2008). Dust particles influence the weather and climate directly through absorbing and scattering the radiation and thereby perturb the Earth's energy balance (direct effect; IPCC, 2013). They also pose indirect effects on the Earth system by modifying the cloud properties and ecosystems (IPCC, 2013). The magnitude of these effects varies with the abundance of the dust particles in the atmosphere and their physicochemical properties such as size distribution, composition, and shape (Mahowald et al., 2014; Shao et al., 2011). Despite of the significant progress made by individual studies, there are still open questions with respect to dust emission/removal processes as well as the size distribution and, consequently, its atmospheric burden (Ansmann et al., 2017; Cakmur et al., 2006; Kok et al., 2017; Shao et al., 2011). Besides, the optical properties of dust constitute a major source of uncertainty in atmospheric models (Tegen, 2003).

The optical properties of dust not only depend on the size and composition (Kandler et al., 2007) but also vary significantly with the shape of the particles (Nousiainen & Kandler, 2015). Mineral dust particles are known as exclusively nonspherical particles with irregular shapes and surface heterogeneity (Reid, 2003; Wagner et al., 2012; Wiegner et al., 2009). Several studies have shown that modeling the dust optical properties based on the spherical model, a usual simplification to circumvent modeling and computational difficulties, leads to large errors in modeling and remote sensing applications (Dubovik et al., 2002; Kahn et al., 1997; Kalashnikova & Sokolik, 2004; Kok et al., 2017; Nousiainen, 2009). To overcome this limitation, several

Investigation: G. A. Hoshyaripour, V. Bachmann, J. Förstner, A. Steiner, H. Vogel, B. Vogel
Project Administration: H. Vogel, B. Vogel
Resources: H. Vogel, B. Vogel
Supervision: B. Vogel
Visualization: G. A. Hoshyaripour, V. Bachmann, A. Steiner, F. Wagner
Writing - review & editing: G. A. Hoshyaripour, V. Bachmann, J. Förstner, A. Steiner, H. Vogel, F. Wagner, B. Vogel

nonspherical particle models and the relevant computational techniques have been developed and deployed to analyze and reproduce the experimental data (see Nousiainen & Kandler, 2015, and references therein).

Among all models ranging from simplified homogeneous to complex anisotropic and inhomogeneous particles, triaxial ellipsoids can closely reproduce the laboratory-measured scattering properties of dust and are therefore recommended for further applications (Dubovik et al., 2006; Meng et al., 2010; Merikallio et al., 2013; Nousiainen & Kandler, 2015). As a pioneer study, Dubovik et al. (2002) applied the randomly oriented polydisperse spheroids (ellipsoids with rotational symmetry) to angular and spectral radiation measurements from the Aerosol Robotic Network (AERONET). They demonstrated a significant improvement in dust-particle phase functions, size distributions, and refractive indices in comparison to Mie-based retrievals. Later, it was shown that utilizing mixtures of spheroids improves the fitting of measured spectral and angular dependencies of intensity and polarization observed by AERONET ground-based Sun/sky radiometers (Dubovik et al., 2006). In radiative transfer models, it has been shown that accounting for ellipsoid dust shapes can lead to changes in top of atmosphere fluxes of up to 30% (Yi et al., 2011). In general circulation models, the role of nonspherical dust shape has been controversial. For instance, Raisanen et al. (2013) suggested that the dust nonsphericity has a minor impact on radiative fluxes and heating rates, hence a generally negligible climate effect. On the other hand, Colarco et al. (2014) reported that for the spheroid dust particles, the effects are more pronounced with changes by 20% and 10% in shortwave and longwave atmospheric heating, respectively. Based on this work, Nowottnick et al. (2015) suggested that the particles shape should be considered in the evaluation of aerosol types in global models. Beside radiation, particle shape affects the dust terminal velocity and, thus, its mass concentration and size distribution. However, Ginoux (2003) showed that such effects are rather negligible in global modeling.

Several experimental and remote sensing studies have shown that any reasonable distribution of nonspherical particles is superior compared to the spherical particles used by Mie theory when it comes to optical properties of mineral dust (see Nousiainen, 2009, and references therein). Especially, the dust nonsphericity is extensively studied and applied in lidar investigations (e.g., Ansmann et al., 2017; Gaststeiger et al., 2011; Jeong et al., 2016; Kemppinen et al., 2015). However, dealing with nonsphericity is not a completely resolved issue in dust forecast models as most models are still based on the Mie theory. In particular, it is not yet clear if accounting for dust nonsphericity enhances the agreement between the modeled and observed scattering in terms of magnitude (e.g., optical depth) and angular distribution (e.g., attenuated backscatter [ABS]). This matter becomes crucial in the data assimilation applications, where model and observation (e.g., satelite, lidar, and ceilometer) should rely on similar physical assumptions concerning the aerosol optical properties. The current study aims to address this issue through investigating the impact of particle shape on the optical depth and ABS simulated by an online-coupled forecasting system. The analysis focuses on North Africa as the most significant dust source globally (Textor et al., 2006). It also accounts for the major source of dust outbreaks reaching Europe. Section 2 describes the tools, methods, and assumptions employed to model the dust radiative effect as well as the observations of dust optical depth and ABS used to evaluate the modeling results. The results are discussed in section 3, and the conclusions are given in section 4. It should be noted that this study focuses on the effect of nonsphericity on model-observation comparison and thus does not analyze the effects of particle shape on radiative fluxes and heating rates.

2. Methodology

2.1. Modeling System

This study employs the ICOsahedral Nonhydrostatic weather and climate model with Aerosols and Reactive Trace gases (ICON-ART). ICON is a nonhydrostatic modeling system that solves the full three-dimensional nonhydrostatic and compressible Navier-Stokes equations on an icosahedral grid (Zängl et al., 2015). ICON is a multiscale unified numerical weather prediction and climate modeling system that could be used for seamless simulations of various processes across local to global scales. The ART module is an extension of ICON to account for emission, transport, and physicochemical processing of the aerosols and trace gases (Rieger et al., 2015). Zängl et al. (2015) and Rieger et al. (2015) provide detailed technical descriptions of ICON and ICON-ART, respectively.

ART uses a modal aerosol microphysics model (Rieger et al., 2015). The size distribution of mineral dust at emission is represented by three log-normal modes with mass median diameters of 1.5, 6.7, and 14.2 μm and standard deviation of 1.7, 1.6, and 1.5 for modes A, B, and C, respectively. The dust emission scheme is based on Vogel et al. (2006). It is further improved by Rieger et al. (2017) to consider (1) the global availability of soil

properties (size distribution and residual soil moisture), (2) the soil dispersion state, and (3) a tile approach used to account for soil type heterogeneity at coarse resolutions. The partitioning of the emitted dust in different modes depends on wind velocity (Vogel et al., 2006). The dust removal processes include dry (by gravitational settling and turbulent diffusion) and wet deposition (due to washout). Detailed information about the dust cycle in ICON-ART is given in Vogel et al. (2006), Gasch et al. (2017), and Rieger et al. (2017). It should be noted that this study considers the effect of nonsphericity only on dust optical properties. This means the impacts of nonsphericity on dust emission, transport, and removal processes are beyond the scope of this work.

ICON makes use of the Rapid Radiative Transfer Model (RRTM; Mlawer et al., 1997) as the standard radiation scheme for numerical weather prediction. To account for the dust radiative effect, ART calculates the local radiative transfer parameters based on the optical properties and the prognostic mass concentration of dust at every grid point and for every level. These are subsequently used as the input parameters for the RRTM scheme (Gasch et al., 2017). This approach ensures full coupling and feedback between dust processes, radiation, and the atmospheric state (Shao et al., 2011). Furthermore, in this study the dust composition is assumed to be spatially invariant.

Measurements of Aerosol Optical Depth (AOD) and ABS represent the intensity and backward distribution of the scattering by aerosols, respectively (Petty, 2006). To allow a direct comparison between the measurements and modeling results, two forward operators are implemented in ICON-ART to diagnose the AOD and ABS at different wavelengths. These forward operators take the prognosed particle mass concentration and multiply it by the mass extinction and backscatter coefficients that are calculated as explained in the following section.

2.2. Calculation of Dust Optical Properties

Two sets of aerosol optical properties are calculated off-line for each dust mode in ICON-ART. The first set includes the mass extinction coefficient, single scattering albedo, and asymmetry parameter at 30 wavelength bands in the range of 0.2 to 100 μm required by the RRTM scheme to account for the radiative feedback of the dust. The second set includes the mass extinction coefficient (at 550 nm) and the backscatter coefficient (at 532 and 1,064 nm) required for the forward operators to calculate the AOD and ABS, respectively.

The calculation of the optical properties is based on the wavelength-dependent refractive indices of dust used by Rieger et al. (2017), which is in good agreement (difference <5% in the shortwave) with the recent dust refractive index databases for North Africa (Stegmann & Yang, 2017). For spherical particles, the results of the Mie calculations conducted by Gasch et al. (2017) are used. The optical properties of nonspherical particles are based on the database of single scattering properties of randomly oriented triaxial ellipsoids compiled by Meng et al. (2010). This database is developed using the T-Matrix method (Mishchenko et al., 1996) for spheroids. It also uses the Discrete Dipole Approximation and Improved Geometric Optics Method for triaxial ellipsoids without rotational symmetry and also for spheroids with extreme aspect ratio (see Meng et al., 2010, for more details). This database has limitations in accurately simulating the backscatter (Meng et al., 2010). Databases that assume irregularly shaped particles and inhomogeneous distribution of chemical components (e.g., Gaststeiger et al., 2011; Kemppinen et al., 2015; Jeong et al., 2016) seem more accurate in this case. However, such databases have limited range of size parameter (measure of particle radius: wavelength ratio). This means that they are appropriate for the forward operator of ABS (diagnostic calculations) but do not cover the wide size parameter range required for RRTM input parameters (prognostic calculations). Therefore, to have consistent shape assumptions in prognostic and diagnostic calculations in the model, the Meng et al. (2010) database is used for both parts in this study.

The extinction efficiency q_{ext}, the scattering efficiency q_{sca}, and the first element (P_{11}) of the scattering matrix $\mathbf{P}(\theta)$ are taken from Meng et al. (2010) for given wavelength λ, particle shape, and refractive index. The mass extinction coefficient (σ_{ext}) and backscatter coefficient (β) for particle radius r (or volume-equivalent radius for nonspherical particles) are calculated as follows (Petty, 2006):

$$\sigma_{\text{ext}} = \frac{\int_{r_{\min}}^{r_{\max}} \pi r^2 q_{\text{ext}}(r) n(r) dr}{\int_{r_{\min}}^{r_{\max}} \frac{4}{3} \rho \pi r^3 n(r) dr}, \tag{1}$$

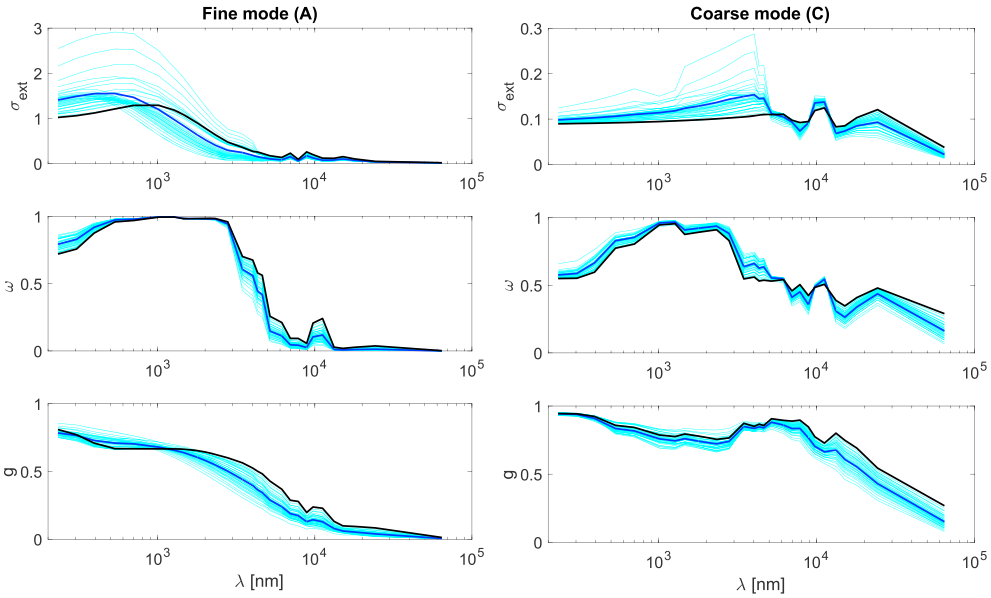

Figure 1. Mass extinction coefficient (σ_{ext}) in square meters per gram (top panel), single-scattering albedo (ω; middle panel), and asymmetry parameter (g; lower panel) of the dust particles in fine (left panel) and coarse (right panel) modes as a function of wavelength (λ). Cyan lines represent 35 different ellipsoids with the average shown by the thick blue line. Black line stands for spherical particles (Mie theory).

$$\beta = \frac{\int_{r_{min}}^{r_{max}} \pi r^2 q_{sca}(r) \frac{P_{11}(r,\pi)}{4\pi} n(r) dr}{\int_{r_{min}}^{r_{max}} \frac{4}{3} \rho \pi r^3 n(r) dr}, \quad (2)$$

where $n(r) = dN/dr$ is the particle number density per radius interval and ρ is the density of dust. β is used together with the two-way transmittance to calculate the ABS as $\beta' = \beta \times exp(-2\tau)$ where τ is the optical depth. In other words, to calculate the mass extinction and backscatter coefficients, σ_{ext} and β are integrated over each log-normal mode, respectively. This procedure is applied to all nonspherical particles in Meng et al. (2010) database that includes 35 ellipsoids with and without rotational symmetry having axis ratios of 1.1 to 3.3 (in agreement with range proposed by Kandler et al., 2007). Then, the average of each optical parameter is calculated and implemented in ICON-ART. This implies the assumption that the shapes have equal weight percents (approximately 3 wt%) in each mode to avoid bias to one particular shape or axis ratio. This assumption is in agreement with the experimental studies that report no significant trend in the aspect ratio and shape as function of particle size (Scheuvens & Kandler, 2014).

The results are shown in Figures 1 and 2 and are compared with the results for volume-equivalent spheres. Figure 1 indicates that in the visible band, nonspherical dust tends to have higher extinction (top panel) and scattering (middle panel) than spherical dust, which is in agreement with previous works (Colarco et al., 2014; Dubovik et al., 2002). It also shows that the extinction coefficient is highly sensitive to the choice of shape and aspect ratio. Thus, using only one shape or aspect ratio might lead to significant overestimation of AOD. Figure 2 shows the phase function at 1,064 nm. Note that in equation (2), the values of $P_{11}(\pi)$ are used to calculate the backscatter coefficient for different modes. It could be seen that the $P_{11}(\pi)$ values for the fine mode (mode A) do not change significantly with shape. But in the coarser modes, the differences in $P_{11}(\pi)$ are up to the order of 10^2.

Dubovik et al. (2006) proposed a mixture of spheroids with shape distribution to represent the dust non-sphericity. The phase function for this distribution (Dubovik et al., 2006) is computed based on Meng 2010 data and shown in Figure 2 (dashed green line). It could be seen that the overall difference between equally weighted ellipsoids mixture (this study) and the spheroid mixture based on shape distribution of Dubovik et al. (2006) is negligible. Besides, the $P_{11}(\pi)$ differs by 5–20% between the ellipsoid and spheroid mixtures that could be neglected too considering the uncertainties associated with both databases (Dubovik et al., 2006; Meng et al., 2010).

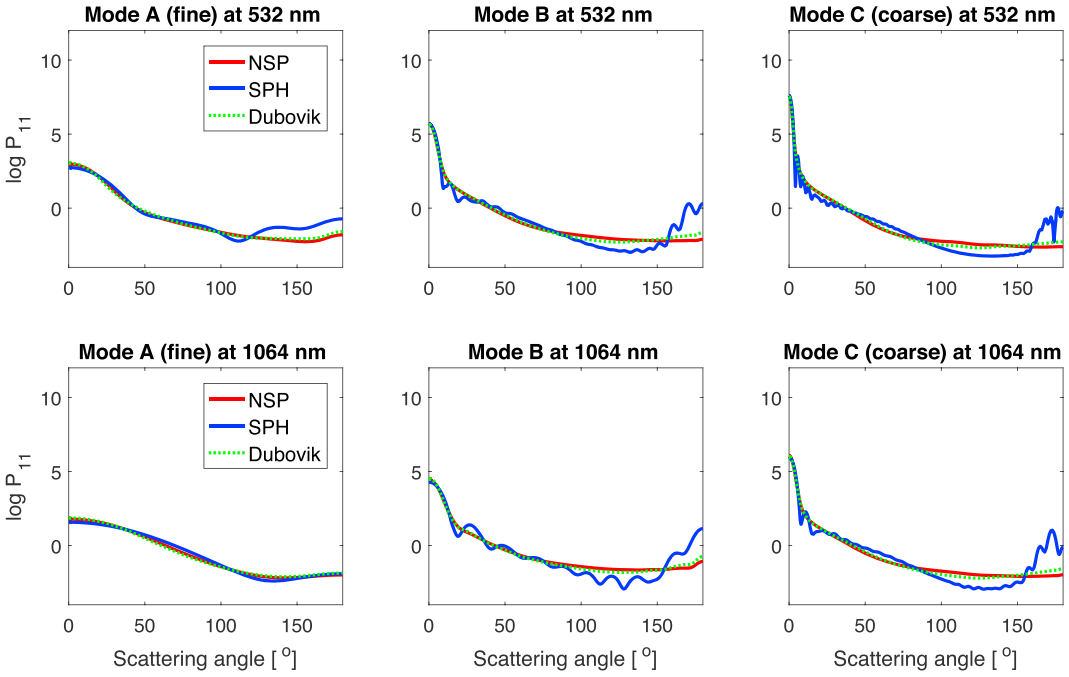

Figure 2. Scattering phase function at wavelengths 532 and 1,064 nm for SPH (blue) and NSP (red) particles in all size modes. Dashed green line is based on the spheroid shape distribution proposed by Dubovik et al. (2006). SPH = spherical; NSP = nonspherical.

It should be noted that in this study shape refers to optical shape and not geometric shape. In other words, the objective is to reproduce the optical behavior of dust particles by a generic combination of nonspherical shapes without considering the geometric shapes of particles observed in particular dust samples.

2.3. Modeling Experiment Setup

The simulations are carried out on a global R2B06 grid with an effective horizontal grid spacing of 40 km and 90 vertical levels. A series of daily forecasts with lead times up to 72 hr is computed for the time period of 15 June 2017 to 31 August 2017. The first 2 weeks are regarded as spin-up time; hence, the evaluation focuses on July and August 2017. The forecasts are initialized daily at 00 UTC based on the initial meteorological conditions taken from a daily analysis provided by the German Weather Service (DWD). The initial mineral dust distributions, however, are taken from the previous forecast run.

The model configuration only treats dust as prognostic aerosol and uses climatology for other aerosols. Prognostic dust-cloud interactions are not taken into account. Furthermore, the linear scaling parameter C_{white} (Rieger et al., 2017), which adjusts the dust emission flux, was tuned with regard to the applied horizontal resolution, yielding a value of $C_{\text{white}} = 0.3$. To assess the impact of particle nonsphericity on diagnosed AOD and ABS, two experiments are carried out. The reference experiment (referred to as SPH) is based on the optical properties of the spherical particles, while the second experiment (referred to as NSP) uses the optical properties for nonspherical shapes, as explained in section 2.2.

The prognostic mineral dust-radiation interactions are activated for both experiments. This implies that the differences between experiments (in diagnosed AOD and ABS) are induced by the changes in optical properties as well as the changes in mineral dust concentrations due to the nonlinear feedback mechanisms in each experiment (e.g., for reduction in dust emission due to modified atmospheric conditions). This effect is quantified and considered in the analysis presented below.

2.4. Observation Data

Three observational data sets are used to evaluate the model simulations (Table 1) that do not use Mie theory as a priori in the retrieval algorithm. The spatial distributions of AOD are taken from the Multiangle Imaging Spectroradiometer (MISR) level 2 and mapped to the spatial resolution of 0.5° (Kahn et al., 2010). MISR provides the nonspherical AOD fraction that could be attributed to dust with high confidence (Guo et al., 2013; Kahn et al., 2009; Kalashnikova & Kahn, 2006). In addition, the total coarse-mode AOD (version 3,

Table 1
Observational Data Sets Used to Evaluate the Model Simulations in This Study

Sensor/platform	Data products	Scope of use	Reference
MISR	AOD (total and nonspherical)	Spatial distribution	Kahn et al. (2010)
CALIPSO	ABS	Vertical profiles	Winker et al. (2013)
AERONET	Coarse-mode AOD	Temporal variation	Dubovik et al. (2002)

Note. MISR = Multiangle Imaging Spectroradiometer; AOD = Aerosol Optical Depth; CALIPSO = Cloud-Aerosol Lidar and Infrared Pathfinder Satellite Observation; AERONET = Aerosol Robotic Network; ABS = Attenuated Backscatter.

level 1.5) from ground-based AERONET is used to evaluate temporal variations of the simulated AOD. The coarse mode AOD is also dominated by mineral dust (O'Neill et al., 2003). The AOD retrieval in this data set is based on the spectral deconvolution algorithm described in O'Neill et al. (2003). Six AERONET sites in the study region are considered, including two inland sites in North Africa (Tamanrasset and Banizoumbou), two coastal sites in North Africa (Dakar and Tizi-Ouzou), one island site in Mediterranean sea (Lampedusa), and one inland site in Europe (Zaragoza).

The vertical profiles of the aerosols are taken from the Cloud-Aerosol Lidar with Orthogonal Polarization sensor onboard of Cloud-Aerosol Lidar and Infrared Pathfinder Satellite Observation (CALIPSO) satellite (Winker et al., 2009). The lidar backscatter profiles are calibrated and range registered to identify the cloud and aerosol layers and also to retrieve aerosol extinction coefficients and ABS at 1,064 nm (Winker et al., 2013). Here the L1B data of the release version 3.40 are used.

All the model-data comparisons are performed with matching the sampling time (for both satellite overpass and AERONET) and also considering the missing data. This approach reduces the artifacts in the observed differences between model and data. It should be noted that the goal of the comparison is not to obtain an exact match with a specific datum but rather to enhance the ability to reproduce the overall variations and features, given the uncertainties in both model and observations.

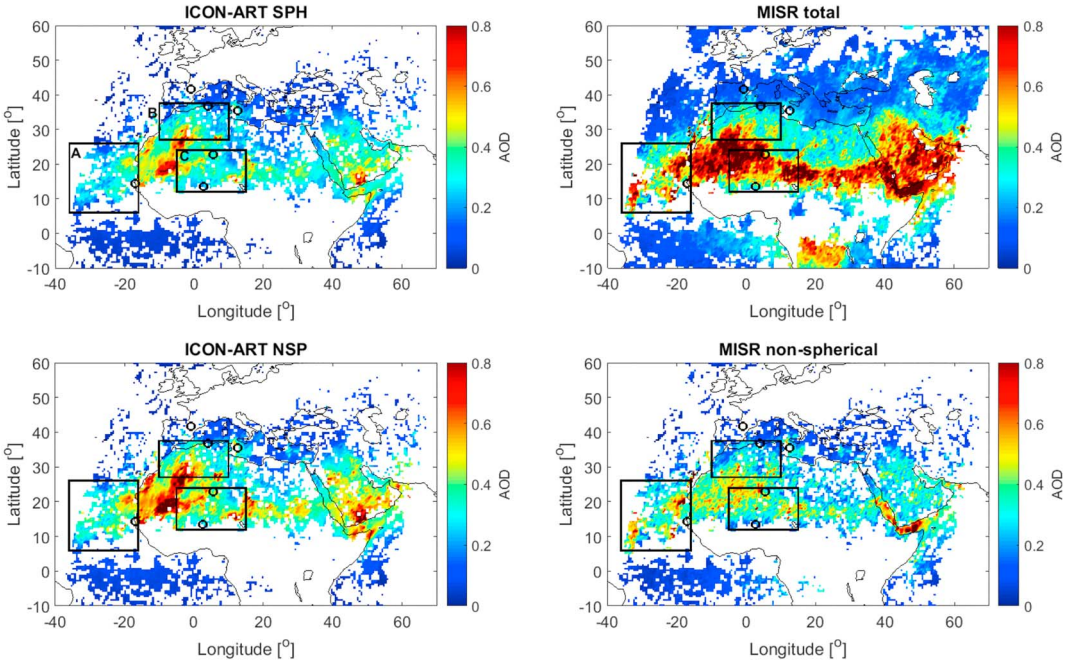

Figure 3. Mean monthly Aerosol Optical Depth at 550 nm for July 2017 calculated from modeling experiments and MISR products. Box A shows the area where MISR nonspherical Aerosol Optical Depth has lower uncertainty. Boxes B and C include major dust source areas in northern and southern Sahara, respectively. These boxes are further analyzed in Figure 4. Circles show the Aerosol Robotic Network stations that are analyzed in section 3.2. ICON-ART = ICOsahedral Nonhydrostatic weather and climate model with Aerosols and Reactive Trace gases; MISR = Multiangle Imaging Spectroradiometer; SPH = spherical; NSP = nonspherical.

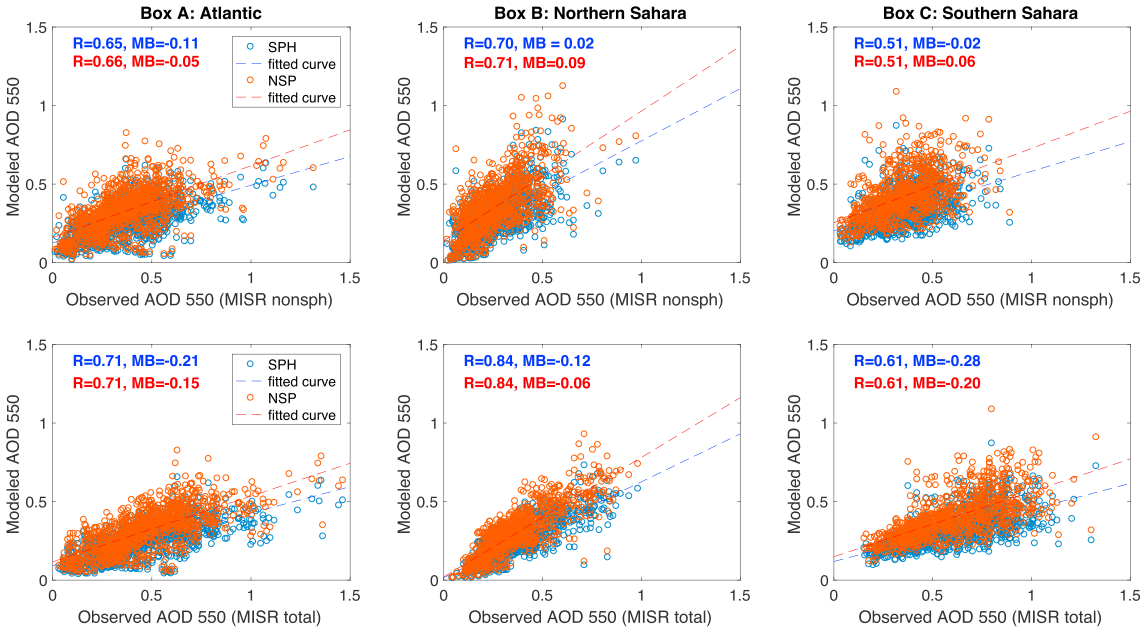

Figure 4. Effect of shape on ICOsahedral Nonhydrostatic weather and climate model with Aerosols and Reactive Trace gases and MISR AOD 550 comparison within the marked areas in Figure 3 for July 2017. MISR nonspherical AOD and MISR total AOD are used in upper and lower panels, respectively. Left, middle, and right panels correspond to boxes A, B, and C in Figure 3, respectively. MISR = Multiangle Imaging Spectroradiometer; AOD = Aerosol Optical Depth; SPH = spherical; NSP = nonspherical.

3. Results and Discussion

3.1. Spatial Distribution of AOD

To allow a detailed analysis, three regions are considered within the study area (boxes A–C in Figure 3). Box A focuses on the dust plumes over the Atlantic ocean where satellite products are more reliable (Kahn & Gaitley, 2015, see below for more explanations). Boxes B and C include the major dust source regions in northern and southern Sahara that contribute mainly to the dust events reaching Europe and Atlantic, respectively (Ginoux et al., 2012). These boxes also include some of the AERONET stations considered in this study (circles in Figure 3).

Figure 3 shows the monthly mean AOD at 550 nm calculated from the modeling experiments and the MISR products. In general, the NSP experiment shows higher AOD compared to SPH experiment as the extinction coefficients of the nonspherical particles at 550 nm are 15–28% larger than those of equivalent spheres (see Figure 1). This is mainly caused by the greater surface-to-volume ratio of nonspherical dust, relative to that of an equal-volume sphere. Both experiments, however, show larger AOD values than the MISR nonspherical AOD. MISR has limitations in the aerosol type retrieval, not only due to limited information in the observed radiances but also due to limitations in the retrieval algorithm. With respect to the observations, at low AOD, or when the surface is very bright, there is little or no information about particle type in the radiances, even if AOD can be retrieved (Kahn & Gaitley, 2015). Regarding the retrieval algorithm, there is a lack of appropriate optical models for the coarse mode mineral dust (Kahn et al., 2010). Both of these limitations become very important over North Africa where the surface is bright and the coarse mode is dominant. This is also visible if one compares the nonspherical AOD with the total AOD of MISR in Figure 3. Indeed, MISR attributes less than 50% of the AOD to nonspherical particles (dust) over the major dust sources in North Africa. This is not the case over the Atlantic (box A in Figure 3) where the dark surface and medium mode dust are dominant (although sea salt contributes to the total AOD). As a result, over the ocean, the MISR nonspherical AOD could be attributed to dust with more certainty compared to the over-land products (Kahn & Gaitley, 2015). Considering this, the NSP experiment in Figure 3 better reproduces the intensity and extension of the plume over the North Atlantic. This area is further analyzed in Figure 4 (box A; upper panel, left) where the modeled AOD and the MISR nonspherical AOD are compared. Indeed, the enhancement of regression coefficient (R) is negligible, whereas the mean bias (MB) is halved in NSP experiment. Thus, there is an enhanced agreement between the NSP experiment and MISR nonspherical AOD in this area.

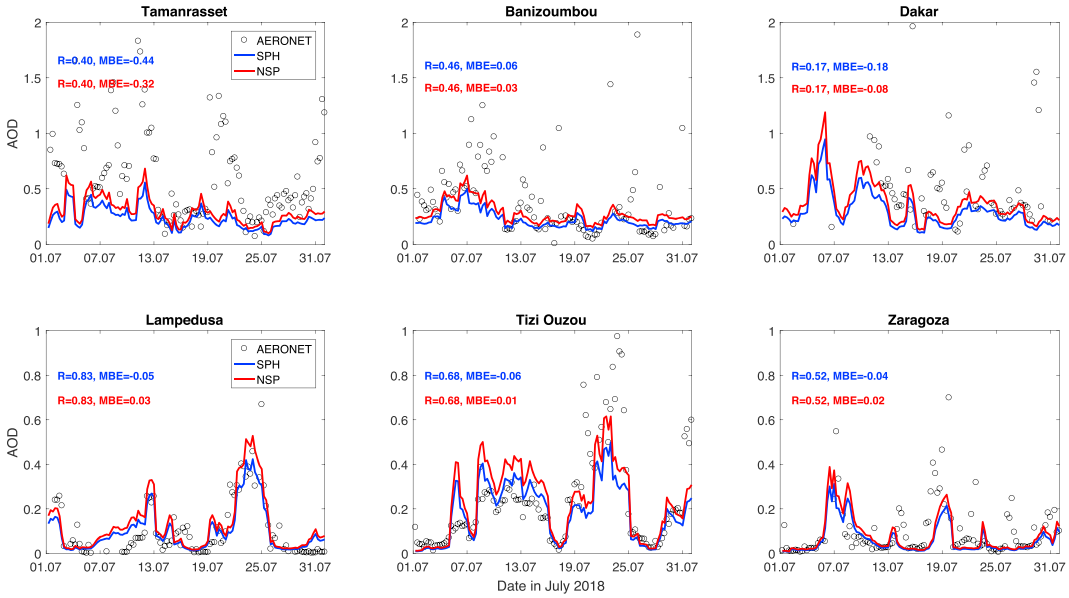

Figure 5. Three-hourly AOD of July 2017 at six AERONET stations shown in Figure 3. Results are obtained from modeling experiments (SPH blue and NSP red) for AOD at 550 nm and AERONET coarse mode measurements at 500 nm. AOD = Aerosol Optical Depth; AERONET = Aerosol Robotic Network; SPH = spherical; NSP = nonspherical.

Two major dust source regions in northern and southern Sahara (boxes B and C in Figure 3) are also analyzed in Figure 4. Given the uncertainties of MISR nonspherical AOD over Sahara discussed above, it is difficult to make a robust interpretation of the boxes B and C in the upper panel of Figure 3. Nevertheless, if one compares, although with caution, both SPH and NSP experiments with MISR total AOD (boxes B and C in the lower panel of Figure 4), it seems that the model generally underestimates the AOD over the source regions. There is a better agreement between the model results and MISR observations (total AOD) in the northern Sahara (box B) than those in the south (box C). This might have implications for the sites located downwind these source areas and, thus, is further investigated using the AERONET data in the following section.

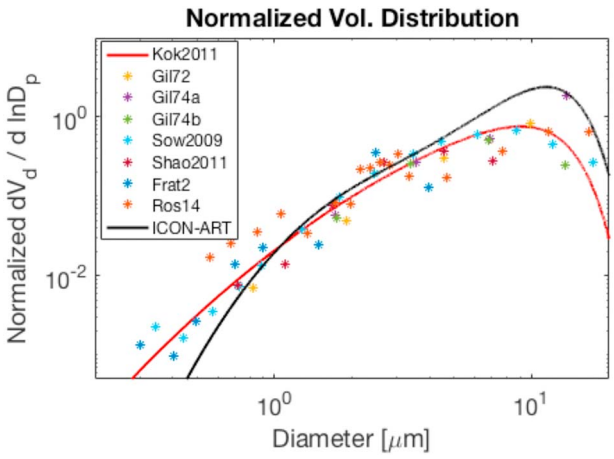

Figure 6. Normalized volume distribution of the emitted dust in ICON-ART (black line) and as the theoretical model of Kok (2011). Dots show the in situ measured dust particle size distribution at emission. Shown are measurements from Gill72 (Gillette et al., 1972), Gill74a (Gillette, 1974), Gill74b (Gillette et al., 1974), Sow2009 (Sow et al., 2009), Shao2011 (Shao et al., 2011), Frat2 (Fratini et al., 2007), and Ros14 (Rosenberg et al., 2014). Adopted from Kok et al. (2017). ICON-ART = ICOsahedral Nonhydrostatic weather and climate model with Aerosols and Reactive Trace gases.

3.2. Temporal Variation of AOD

Data from AERONET stations are used to evaluate the temporal variation of AOD. Figure 5 compares the 3-hourly AOD from model and observations. In general, the impact of the nonsphericity on the temporal variation of the AOD seems to be negligible (correlation coefficient *R* does not change between experiments) although the absolute values of AOD increase in the NSP experiment, which leads to a reduction of the mean bias. The increased AOD indicates the higher extinction of NSP due the greater surface-to-volume ratio compared to that of an equal-volume sphere. Besides, it could be seen that close to the source regions in southern Sahara (Tamanrasset and Banizoumbou in Figure 5), there is less agreement between model and observations compared to the station in the north (Tizi-Ouzou) and also distant sites from the dust sources (Zaragoza and Lampedusa in Figure 5). Dakar shows the least model-observation correlation mainly because the dust particles at this site are mainly originated from the sources in southern Sahara that are underestimated in the model. Thus, the AOD peaks could not be captured. Moreover, sea salt contribution to the AERONET AOD might become significant at this site during the low dust periods. This can explain the discrepancies at this particular site during both low and high AOD periods.

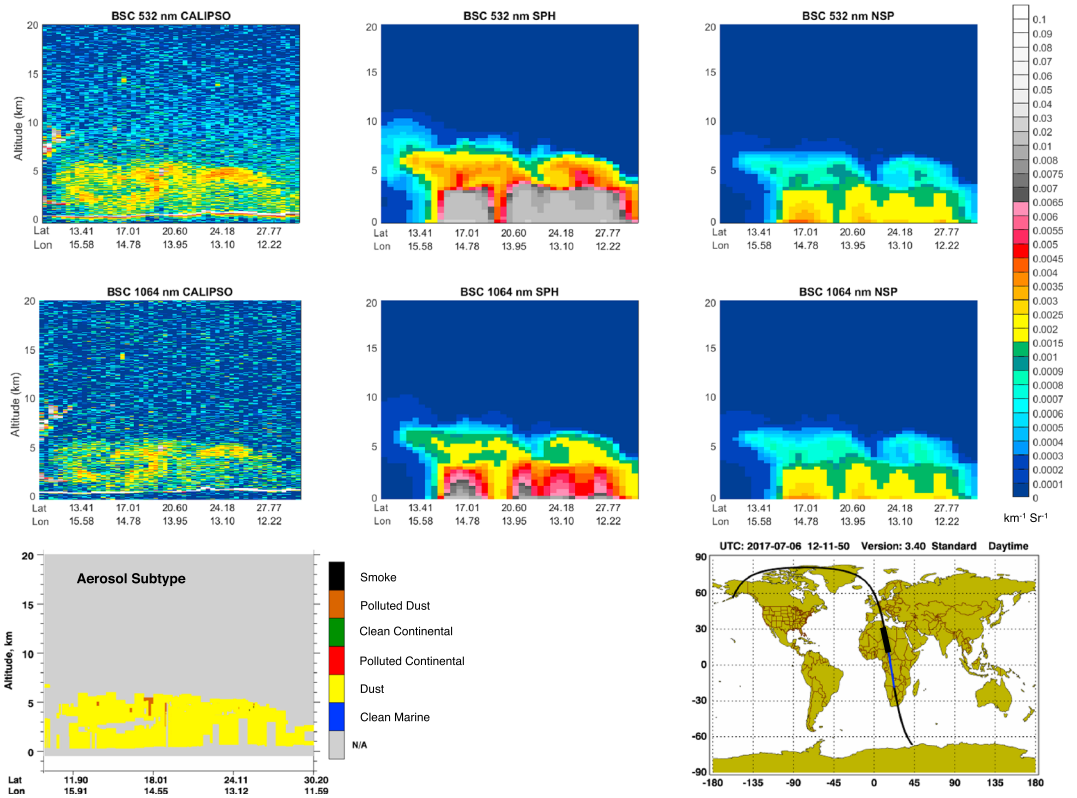

Figure 7. Attenuated Backscatter (at 532 and 1,064 nm) profiles on 6 July 2017 from CALIPSO and modeling experiments. The bottom panel shows the CALIPSO overpass and the aerosol subtypes adopted from CALIPSO website. CALIPSO = Cloud-Aerosol Lidar and Infrared Pathfinder Satellite Observation; SPH = spherical; NSP = nonspherical.

The result presented in Figure 5 are in agreement with those shown in previous section and Figures 3 and 4. To understand the reason of the discrepancy between modeled and observed AOD, one should consider the fact that AOD is a linear function of particle mass concentration and mass extinction coefficient at different size modes. In the midvisible wavelengths, the fine mode has significantly higher extinction coefficient than the coarse mode (a factor of 12–15 according to Figure 1). Thus, underestimation of the fine mode close to source regions can lead to significantly lower AOD in the model. This seems to be the case in ICON-ART according to Figure 6 where the normalized volume size distribution of the emitted dust particles in ICON-ART is compared with the dust emission flux measurements and theoretical data (Kok, 2011; Kok et al., 2017). The normalization follows the work of Kok, (2011, equation 6 therein) that is based on particle size distribution parameters and the brittle fragmentation theory. The in situ measurement data are also analyzed and homogenized by Kok et al. (2017) to represent the globally averaged dust size distribution at emission. Figure 6 suggests that, in ICON-ART, there is an underestimation of fine and overestimation of coarse mode particles. This explains the discrepancy between the modeled and observed AOD close to source regions in North Africa shown in Figures 3–5.

The underestimation of AOD in the source regions can also partly stem from underestimation of the dust emission flux in these areas. For instance, dust storms caused by convective systems and cold pools substantially contribute to emissions in southern Sahara, where convective organization is supported by shear underneath a midlevel jet (see, e.g., Knippertz, 2014, and references therein). These frequent events are not resolved in the model configuration used in this study. This can lead to significant underestimation of dust emission flux and airborne mass concentrations (Gasch et al., 2017) and might partly explain the significant underestimation of the dust episodes (AOD $\geq$ 0.8) in Figure 5.

There are two key sources of uncertainty in the model-AERONET comparison. First, in coastal areas, the contribution of sea-salt particles to AOD might become important. As the model simulates the dust AOD only, some of the discrepancy during low-dust periods (e.g., at Dakar in Figure 5) might be due to this point. Second, fine dust particles contribute to the total extinction too. Thus, the AERONET coarse mode AOD

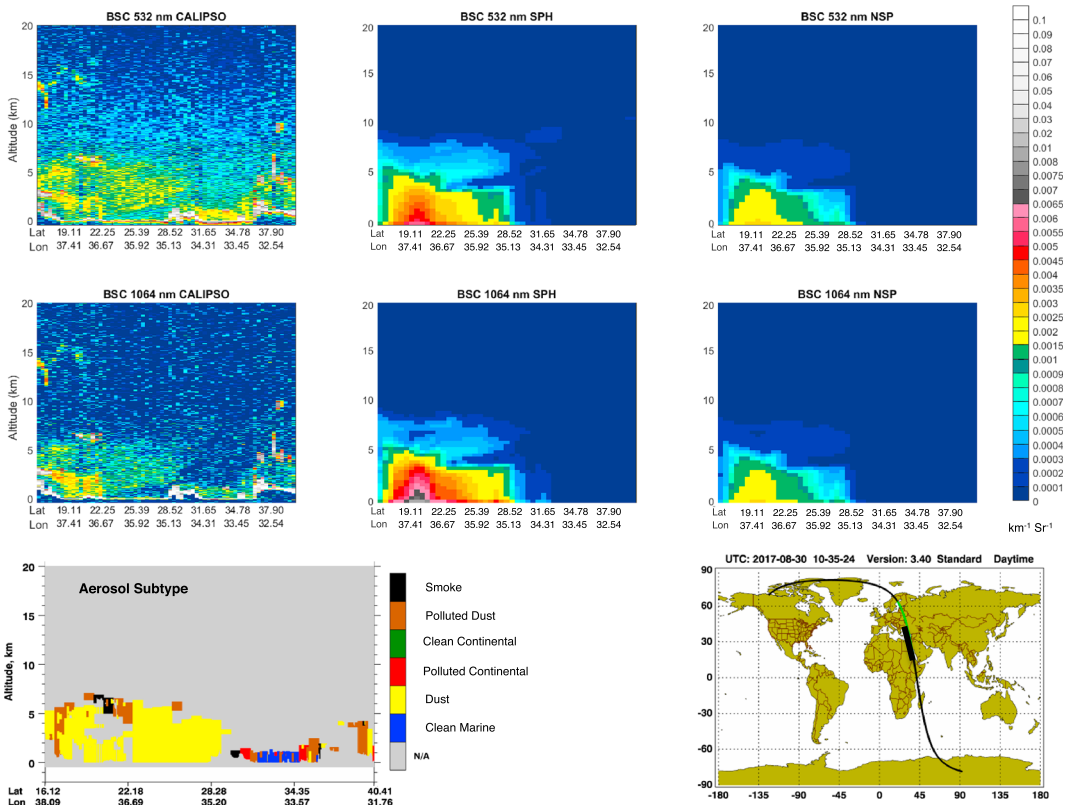

Figure 8. Attenuated Backscatter (at 532 and 1,064 nm) profiles on 30 August 2017 from CALIPSO and modeling experiments. The bottom panel shows the CALIPSO overpass and the aerosol subtypes adopted from CALIPSO website. CALIPSO = Cloud-Aerosol Lidar and Infrared Pathfinder Satellite Observation.

might underestimate the dust AOD especially in the distant sites where fine mode is more dominant (e.g., at Lampedusa in Figure 5).

Accounting for nonsphericity halves the modeled AOD biases but does not significantly improve the model-observation agreement with respect to temporal variability. It seems that the particle size distribution and emission fluxes are more important than the particle shape when it comes to the temporal variations of AOD, especially in the source regions. Nevertheless, improving the dust size distribution and emissions in the modeling system is beyond the scope of this work.

3.3. Vertical Profiles of ABS

Beside the extinction efficiency, particle shape also affects the angular distribution of the scattering. To investigate this effect, vertical profiles of ABS from the model and CALIPSO observations on 6 July 2017 and 30 August 2017 are shown in Figures 7 and 8, respectively. CALIPSO data are resampled at the same resolution as the model to facilitate the direct comparison. According to the aerosol subtype plots, dust is the dominant aerosol species on both dates. Based on the CALIPSO data on 6 July 2017, dust layer lays below 6 km between the latitudes of 10° and 30° N. This layer is very well captured in the NSP experiment. Both horizontal and vertical distributions of the dust layer as well as the intensity of the ABS signal are in a very good agreement with CALIPSO measurements at both 532- and 1,064-nm channels. However, the SPH overestimates the intensity of the observed ABS signal by a factor of 2 to 5 especially close to surface. This is in agreement with the range suggested in lidar studies (Amiridis et al., 2013; Ansmann et al., 2017; Mueller et al., 2007). The same interpretation applies for Figure 8 (30 August 2017), which shows that the dust layer in CALIPSO observation on 30 August 2017 lays below 5 km between the latitudes of 18° and 28° N.

The discrepancy between SPH experiment and observation is more pronounced at 532-nm channel where the ABS is overestimated by factor of 5. This is in agreement with Figure 2 where $P_{11}(\pi)$ (and thus, the backscatter coefficient) of the spherical particles is by up to 2 orders of magnitude larger than the nonspherical ones in all size modes. At 1,064 nm, on the other hand, only coarse modes (B and C) show higher $P_{11}(\pi)$

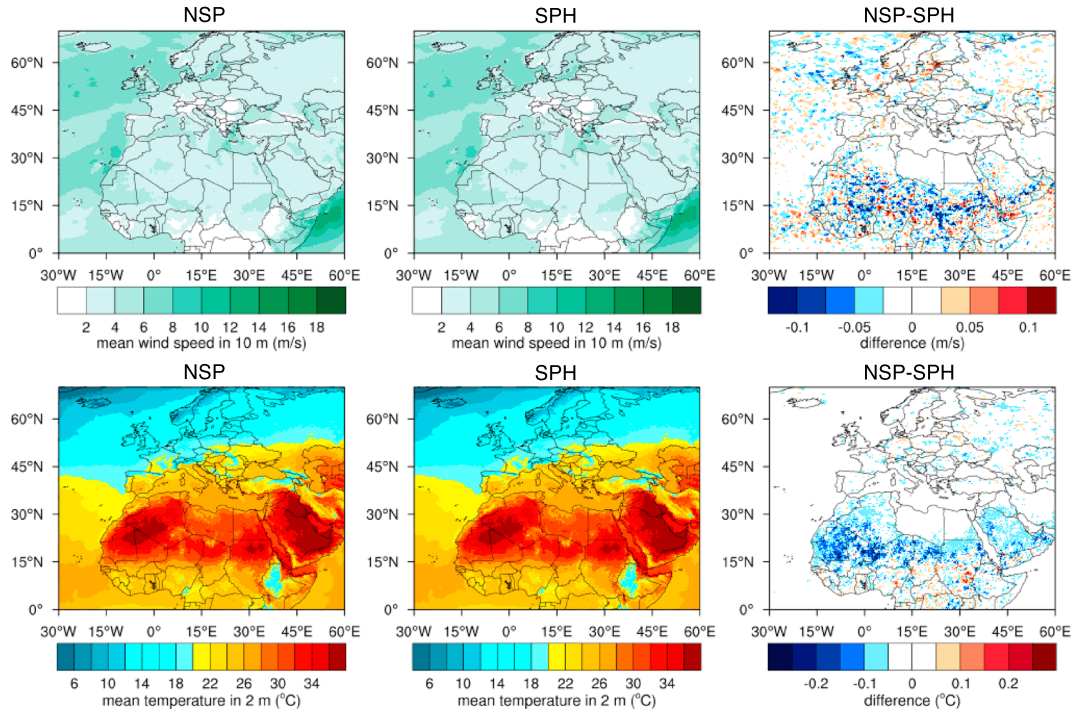

Figure 9. Monthly mean of the third day forecast time for 2-m temperature and 10-m wind speed. All parameters are averaged over July 2017. SPH = spherical; NSP = nonspherical.

values (2 orders of magnitude). Therefore, accounting for nonsphericity leads to significant improvement of the ABS. At 532 nm, the improvements are independent of the size distribution, while at 1,064 nm, the signal enhancements are more pronounced where coarse mode dust is dominant.

3.4. Effect of Dust-Radiative Feedback

As mentioned earlier, a critical aspect of changing the optical properties in the model is that the feedback of radiation to meteorology changes too. In other words, the simulations have different meteorology due to differences in dust radiative forcing. Figure 9 shows the monthly mean of 10-m wind and 2-m temperature in both simulations as well as the differences. Despite of the noise in the southern and northern parts (because of the complex interactions of radiation, clouds, and dynamics), there is a discernible signal over the dust source regions between 10° N and 35° N. The enhanced extinction of nonspherical particles leads to lower temperature and wind in this area. The differences between two simulations are below 1% and 2% for 10-m wind in meters per second and 2-m temperature in degrees Celsius, respectively. These differences affect the dust emission and removal processes and, thus, its airborne mass concentrations. For instance, ±1% change in the wind velocity implies dust emission change by ±3% (as dust emission depends on the third order of wind velocity). This means that the observed differences in the AOD of NSP and SPH experiments are partly related to changes in the extinction coefficient (effect of shape) and partly due to the changes in the dust mass concentration (effect of feedback). To quantify these effects, we assume that any non-zero difference between the mass concentrations implies the contribution of the feedback to AOD differences. When the differences in the dust mass concentration between experiments are below 2%, the differences in AOD are due to the shape only. Based on this assumption, the monthly average of the differences in AOD and the effect of shape on these differences are calculated and shown in Figures 10a and 10b, respectively. Figure 10b shows that more than 90% of the differences in AOD over source regions are related to shape and not feedback. Indeed, in the majority of the areas, where the feedback's contribution is more than 10%, the differences in AOD (Figure 10a) are insignificant. Hence, the analysis and results presented in previous sections are marginally affected by the feedback mechanisms. Based on Figures 10c and 10d, it seems that the coarse mode is mainly affected by the feedbacks on emission and removal processes. This could have implications for the radiative impact of the coarse dust on climate (Kok et al., 2017). However, detailed analysis of these mechanisms is beyond the scope of this work.

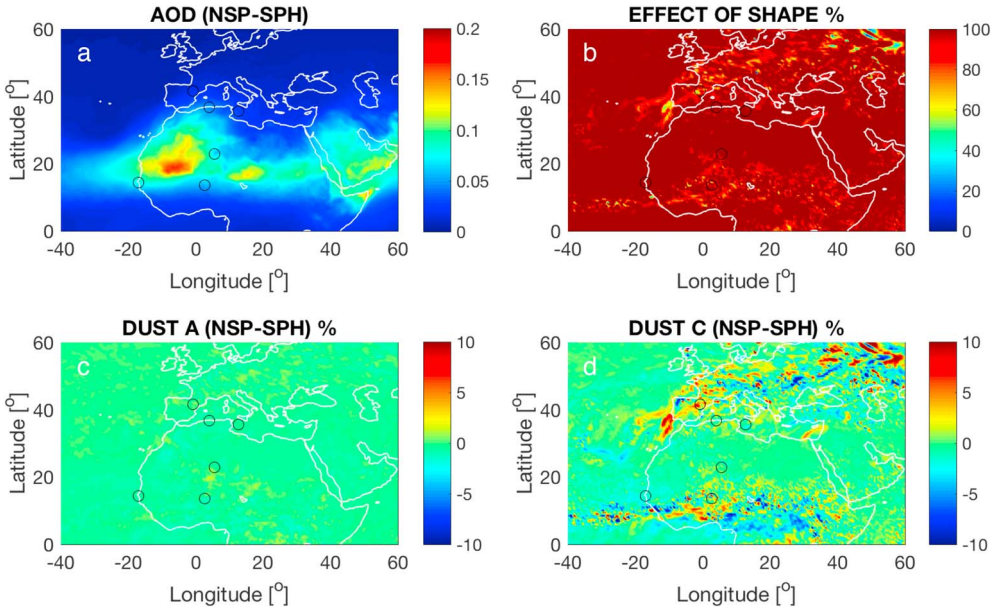

Figure 10. (a) The difference between AOD in NSP and SPH experiments; (b) effect of shape (through extinction coefficient) on changes in AOD; (c) the difference in the mass concentration of fine mode; and (d) the difference in the mass concentration of coarse mode. Note that except AOD, all other values are shown in percent. All parameters are averaged over July 2017. AOD = Aerosol Optical Depth; SPH = spherical; NSP = nonspherical.

4. Summary and Conclusion

This study investigates the impacts of the particle shape on intensity and angular distribution of the light scattering by mineral dust in a dust forecast system and how it affects the model-observation comparison. The optical properties of nonspherical mineral dust particles are calculated assuming a mixture of 35 triaxial ellipsoids and implemented in the online-coupled forecast system ICON-ART. Two numerical experiments are conducted using the optical properties of nonspherical (NSP) and spherical (SPH) particles. The modeling results are evaluated against the AOD observations from MISR and AERONET as well as the ABS measurements from CALIPSO.

The model satisfactorily reproduces the spatial distribution of AOD over North Africa. Accounting for nonsphericity can slightly enhance the agreement between modeled and observed AOD by reducing the model bias, but the overall AOD values (in both NSP and SPH experiments) are lower than MISR observations over North Africa. A similar discrepancy appears in comparison of the model with AERONET observations close to source regions. This stems mainly from two uncertainties in the ICON-ART modeling system: (1) the underestimation of fine mode in the size distribution of the emitted dust and (2) lack of dust emission due to unresolved processes, such as convective systems and cold pools (in particular, over southern Sahara). These two factors eventually lead to underestimation of AOD especially close to the sources in southern Sahara. Thus, for AOD variations, the roles of particle size distribution and emission flux seem to be more important than that of the nonspherical shape.

Vertical profiles of the ABS from model and CALIPSO data are compared during two dust event. Results show that the NSP experiment better reproduces the observed signal. Thus, accounting for nonsphericity improves the agreement between model and observations in case of ABS. Here the particle shape seems to be more important than the size distribution. Hence, the model-observation comparison in case of AOD will only slightly improve by implementation of nonsphericity. On the other hand, its implementation will substantially enhance the model-observation comparison in case of ABS and, thus, should be considered in data assimilation applications.

While the fine mode plays the key role in AOD, the coarse mode is the major player when it comes to ABS. Hence, to improve the agreement between model and observations, representation of both particle shape and size distribution should be improved in the model. The important role of particle size distribution in optical properties of mineral dust is highlighted in several studies (e.g., Huneeus et al., 2011; Maher et al., 2010;

Mahowald et al., 2014, and references therein). It has been shown that a modified representation of mineral dust size distribution in models leads to improvements in the modeled dust cycle and direct effects on the radiative balance (Albani et al., 2014). Therefore, next studies should investigate the sensitivity of the dust cycle and direct effects in ICON-ART modeling system to particle size distribution. It was also briefly mentioned that the modified radiative feedback changes the atmospheric state when particle nonsphericity is considered. Although the implications of these differences are negligible for this work, a detailed study of their effects on atmospheric dynamics and meteorological fields is required.

Acknowledgments
Authors thank Ralph Kahn, Konrad Kandler, Timo Nousiainen, and Jasper Kok for their valuable remarks. The CALIPSO data are obtained from the NASA Langley Research Center Atmospheric Science Data Center. The data can be obtained from KITopen (https://doi.org/10.5445/IR/1000094622). This work is funded by the Federal Ministry for Economic Affairs and Energy and was conducted within the project PerduS: Photovoltaikertragsreduktion durch Saharastaub, 0325932A (Engl. forecasting the reduction in photovoltaic power production during Saharan dust outbreaks). We acknowledge support by Deutsche Forschungsgemeinschaft and open access publishing fund of Karlsruhe Institute of Technology.

References

Albani, S., Mahowald, N. M., Perry, A. T., Scanza, R. A., Zender, C. S., Heavens, N. G., et al. (2014). Improved dust representation in the Community Atmosphere Model. *Journal of Advances in Modeling Earth Systems*, *6*, 541–570. https://doi.org/10.1002/2013MS000279. Received.

Amiridis, V., Wandinger, U., Marinou, E., Giannakaki, E., Tsekeri, A., Basart, S., et al. (2013). Optimizing CALIPSO Saharan dust retrievals. *Atmospheric Chemistry and Physics*, *13*(23), 12,089–12,106. https://doi.org/10.5194/acp-13-12089-2013

Ansmann, A., Rittmeister, F., Engelmann, R., Basart, S., Jorba, O., Spyrou, C., et al. (2017). Profiling of Saharan dust from the Caribbean to Western Africa—Part 2: Shipborne lidar measurements versus forecasts. *Atmospheric Chemistry and Physics*, *17*(24), 14,987–15,006. https://doi.org/10.5194/acp-17-14987-2017

Cakmur, R. V., Miller, R. L., Perlwitz, J., Geogdzhayev, I. V., Ginoux, P., Koch, D., et al. (2006). Constraining the magnitude of the global dust cycle by minimizing the difference between a model and observations. *Journal of Geophysical Research*, *111*, D06207. https://doi.org/10.1029/2005JD005791

Colarco, P. R., Nowottnick, E. P., Randles, C. A., Yi, B., & Yang, P. (2014). Impact of radiatively interactive dust aerosols in the NASA GEOS-5 climatemodel: Sensitivity to dust particle shape and refractive index. *Journal of Geophysical Research: Atmospheres*, *119*, 753–786. https://doi.org/10.1002/2013JD020046. Received.

Dubovik, O., Holben, B. N., Lapyonok, T., Sinyuk, A., Mishchenko, M. I., Yang, P., & Slutsker, I. (2002). Non-spherical aerosol retrieval method employing light scattering by spheroids. *Geophysical Research Letters*, *29*(10), 1415. https://doi.org/10.1029/2001GL014506

Dubovik, O., Sinyuk, A., Lapyonok, T., Holben, B. N., Mishchenko, M., Yang, P., et al. (2006). Application of spheroid models to account for aerosol particle nonsphericity in remote sensing of desert dust. *Journal of Geophysical Research*, *111*, D11208. https://doi.org/10.1029/2005JD006619

Fratini, G., Ciccioli, P., Febo, A., Forgione, A., & Valentini, R. (2007). Size-segregated fluxes of mineral dust from a desert area of Northern China by eddy covariance. *Atmospheric Chemistry and Physics*, *7*(11), 2839–2854. https://doi.org/10.5194/acp-7-2839-2007

Gasch, P., Rieger, D., Walter, C., Khain, P., Levi, Y., Knippertz, P., & Vogel, B. (2017). Revealing the meteorological drivers of the September 2015 severe dust event in the Eastern Mediterranean. *Atmospheric Chemistry and Physics*, *17*, 13573–13604. https://doi.org/10.5194/acp-17-13573-2017

Gaststeiger, J., Wiegner, M., Gross, S., Freundenhalter, V., Toledani, C., Tesche, M., & Kandler, K. (2011). Modelling lidar-relevant optical properties of complex mineral dust aerosols. *Tellus B*, *63*(4), 725–741. https://doi.org/10.1111/j.1600-0889.2011.00559.x

Gillette, D. A. (1974). On the production of soil wind erosion having the potential for long range transport. *Journal de Recherches Atmospheriques*, *8*, 734–744.

Gillette, D. A., Billford, I. H., & Fenster, C. R. (1972). Measurements of aerosol size distributions and vertical fluxes of aerosols on land subject to wind erosion. *Journal of Applied Meteorology*, *11*, 977–987.

Gillette, D. A., Billford, I. H., & Fryrear, D. W. (1974). Influence of wind velocity on size distributions of aerosols generated by wind erosion of soils. *Journal of Geophysical Research*, *79*, 4067–4075.

Ginoux, P. (2003). Effects of nonsphericity on mineral dust modeling. *Journal of Geophysical Research*, *108*(D2), 4052. https://doi.org/10.1029/2002JD002516

Ginoux, P., Prospero, J. M., Gill, T. E., Hsu, N. C., & Zhao, M. (2012). Global-scale attribution of anthropogenic and natural duct sources and their emission rates based on MODIS Deep Blue aerosol products. *Reviews of Geophysics*, *50*, RG3005. https://doi.org/10.1029/2012RG000388. INTRODUCTION.

Guo, Y., Tian, B., Kahn, R. A., Kalashnikova, O., Wong, S., & Waliser, D. E. (2013). Tropical Atlantic dust and smoke aerosol variations related to the Madden-Julian Oscillation in MODIS and MISR observations. *Journal of Geophysical Research: Atmospheres*, *118*, 4947–4963. https://doi.org/10.1002/jgrd.50409

Huneeus, N., Schulz, M., Balkanski, Y., Griesfeller, J., Prospero, J., Kinne, S., et al. (2011). Global dust model intercomparison in AeroCom phase I. *Atmospheric Chemistry and Physics*, *11*, 7781–7816. https://doi.org/10.5194/acp-11-7781-2011

IPCC (2013). *Climate change 2013: The physical science basis. Contribution of Working Group I to the Fifth Assessment Report of the Intergovernmental Panel on Climate Change* (pp. 1535). Cambridge, United Kingdom and New York, NY, USA: Cambridge University Press. https://doi.org/10.1017/CBO9781107415324

Jeong, G. Y., Park, M. Y., Kandler, K., Nousiainen, T., & Kemppinen, O. (2016). Mineralogical properties and internal structures of individual fine particles of saharan dust. *Atmospheric Chemistry and Physics*, *16*(19), 12397–12410. https://doi.org/10.5194/acp-16-12397-2016

Kahn, R., & Gaitley, B. (2015). An analysis of global aerosol type as retrieved by MISR. *Journal of Geophysical Research: Atmospheres*, *120*, 4248–4281. https://doi.org/10.1002/2015JD023322

Kahn, R. A., Gaitley, B. J., Garay, M. J., Diner, D. J., Eck, T. F., Smirnov, A., & Holben, B. N. (2010). Multiangle imaging spectroradiometer global aerosol product assessment by comparison with the aerosol robotic network. *Journal of Geophysical Research*, *115*, D23209. https://doi.org/10.1029/2010JD014601

Kahn, R., Petzold, A., Wendisch, M., Bierwirth, E., Dinter, T., Esselborn, M., et al. (2009). Desert dust aerosol air mass mapping in the Western Sahara, using particle properties derived from space-based multi-angle imaging. *Tellus B: Chemical and Physical Meteorology*, *61*(1), 239–251. https://doi.org/10.1111/j.1600-0889.2008.00398.x

Kahn, R., West, R., Rheingans, B., & Mishchenko, I. (1997). Sensitivity of multiangle remote sensing observations to aerosol sphericity. *Journal of Geophysical Research*, *102*, 16,861–16,870.

Kalashnikova, O. V., & Kahn, R. (2006). Ability of multiangle remote sensing observations to identify and distinguish mineral dust types: 2. Sensitivity over dark water. *Journal of Geophysical Research*, *111*, D11207. https://doi.org/10.1029/2005JD006756

Kalashnikova, O. V., & Sokolik, I. N. (2004). Modeling the radiative properties of nonspherical soil-derived mineral aerosols. *Journal of Quantitative Spectroscopy and Radiative Transfer*, *87*, 137–166. https://doi.org/10.1016/j.jqsrt.2003.12.026

Kandler, K., Benker, N., Bundke, U., Cuevas, E., Ebert, M., Knippertz, P., et al. (2007). Chemical composition and complex refractive index of Saharan Mineral Dust at Izana, Tenerife (Spain) derived by electron microscopy. *Atmospheric Environment*, *41*, 8058–8074. https://doi.org/10.1016/j.atmosenv.2007.06.047

Kemppinen, O., Nousiainen, T., & Jeong, G. Y. (2015). Effects of dust particle internal structure on light scattering. *Atmospheric Chemistry and Physics*, *15*(20), 12,011–12,027. https://doi.org/10.5194/acp-15-12011-2015

Knippertz, P. (2014). Meteorological aspects of dust storms. In P. Knippertz, & J.-B. W. Stuut (Eds.), *Mineral dust: A key player in the Earth system* (pp. 509). Berlin: Springer.

Kok, J. F. (2011). A scaling theory for the size distribution of emitted dust aerosols suggests climate models underestimate the size of the global dust cycle. *Proceedings of the National Academy of Sciences of the United States of America*, *108*(3), 18–20. https://doi.org/10.1073/pnas.1014798108/-/DCSupplemental.www.pnas.org/cgi/doi/10.1073/pnas.1014798108

Kok, J. F., Ridley, D. A., Zhou, Q., Miller, R. L., Zhao, C., Heald, C. L., et al. (2017). Smaller desert dust cooling effect estimated from analysis of dust size and abundance. *Nature Communications*, *10*(April), 274–278. https://doi.org/10.1038/NGEO2912

Maher, B., Prospero, J., Mackie, D., Gaiero, D., Hesse, P., & Balkanski, Y. (2010). Global connections between aeolian dust, climate and ocean biogeochemistry at the present day and at the last glacial maximum. *Earth-Science Reviews*, *99*(1), 61–97. https://doi.org/10.1016/j.earscirev.2009.12.001

Mahowald, N., Albani, S., Kok, J. F., Engelstaeder, S., Scanza, R., Ward, D. S., & Flanner, M. G. (2014). The size distribution of desert dust aerosols and its impact on the Earth system. *Aeolian Research*, *15*, 53–71. https://doi.org/10.1016/j.aeolia.2013.09.002

Meng, Z., Yang, P., Kattawar, G. W., Bi, L., Liou, K. N., & Laszlo, I. (2010). Single-scattering properties of tri-axial ellipsoidal mineral dust aerosols: A database for application to radiative transfer calculations. *Journal of Aerosol Science*, *41*(5), 501–512. https://doi.org/10.1016/j.jaerosci.2010.02.008

Merikallio, S., Nousiainen, T., Kahnert, M., & Harri, A. (2013). Light scattering by the Martian dust analog, palagonite, modeled with ellipsoids. *Journal of the Optical Society of America*, *21*(15), 114–126. https://doi.org/10.1364/OE.21.017972

Mishchenko, M. I., Travis, L. D., & Mackowski, D. (1996). T-matrix computations of light scattering nonspherical particles: A review. *Journal of Quantitative Spectroscopy and Radiative Transfer*, *55*(5), 535–575.

Mlawer, E. J., Taubman, S. J., Brown, P. D., Iacono, M. J., & Clough, S. A. (1997). Radiative transfer for inhomogeneous atmospheres: RRTM, a validated correlated-k model for the longwave. *Journal of Geophysical Research*, *102*(D14), 16,663–16,682. https://doi.org/10.1029/97JD00237

Mueller, D., Ansmann, A., Mattis, I., Tesche, M., Wandinger, U., Althausen, D., & Pisani, G. (2007). Aerosol-type-dependent lidar ratios observed with Raman lidar. *Journal of Geophysical Research*, *112*, D16202. https://doi.org/10.1029/2006JD008292

Nousiainen, T. (2009). Optical modeling of mineral dust particles: A review. *Journal of Quantitative Spectroscopy and Radiative Transfer*, *110*(14-16), 1261–1279. https://doi.org/10.1016/J.JQSRT.2009.03.002

Nousiainen, T., & Kandler, K. (2015). Light scattering by atmospheric mineral dust particles. In T. Nousiainen, & K. Kandler (Eds.), *Light scattering reviews 9* (pp. 3–52). Berlin, Heidelberg: Springer Praxis Books.

Nowottnick, E. P., Colarco, P. R., Welton, E. J., & da Silva, A. (2015). Use of the CALIOP vertical feature mask for evaluating global aerosol models. *Atmospheric Measurement Techniques*, *8*(9), 3647–3669. https://doi.org/10.5194/amt-8-3647-2015

O'Neill, N. T., Eck, T. F., Smirnov, A., Holben, B. N., & Thulasiraman, S. (2003). Spectral discrimination of coarse and fine mode optical depth. *Journal of Geophysical Research*, *108*(D17), 4559. https://doi.org/10.1029/2002JD002975

Petty, G. (2006). *A first course in atmospheric radiation*. Madison, USA: Sundog Pub.

Raisanen, P., Haapanala, P., Chung, C. E., Kahnert, M., Makkonen, R., Tonttila, J., & Nousiainen, T. (2013). Impact of dust particle non-sphericity on climate simulations. *Quarterly Journal of the Royal Meteorological Society*, *139*(October), 2222–2232. https://doi.org/10.1002/qj.2084

Reid, E. A. (2003). Characterization of African dust transported to Puerto Rico by individual particle and size segregated bulk analysis. *Journal of Geophysical Research*, *108*(D19), 8591. https://doi.org/10.1029/2002JD002935

Rieger, D., Bangert, M., Bischoff-Gauss, I., Förstner, J., Lundgren, K., Reinert, D., et al. (2015). ICON-ART 1.0—A new online-coupled model system from the global to regional scale. *Geoscientific Model Development*, *8*(6), 1659–1676. https://doi.org/10.5194/gmd-8-1659-2015

Rieger, D., Steiner, A., Bachmann, V., Gasch, P., Förstner, J., Deetz, K., et al. (2017). Impact of the 4 April 2014 Saharan dust outbreak on the photovoltaic power generation in Germany. *Atmospheric Chemistry and Physics*, *17*(21), 13,391–13,415. https://doi.org/10.5194/acp-17-13391-2017

Rosenberg, P. D., Parker, D. J., Ryder, C. L., Marsham, J. H., Garcia-Carreras, L., Dorsey, J. R., et al. (2014). Quantifying particle size and turbulent scale dependence of dust flux in the Sahara using aircraft measurements. *Journal of Geophysical Research: Atmospheres*, *119*, 7577–7598. https://doi.org/10.1002/2013JD021255

Scheuvens, D., & Kandler, K. (2014). On composition, morphology, and size distribution of airborne mineral dust. In D. Scheuvens, & K. Kandler (Eds.), *Mineral dust: A key player in the Earth system* (pp. 509). Dordrecht: Springer.

Shao, Y. (2008). *Physics and modelling of wind erosion* (pp. 459). Dordrecht: Springer.

Shao, Y., Wyrwoll, K.-h., Chappell, A., Huang, J., Lin, Z., Mctainsh, G. H., et al. (2011). Dust cycle: An emerging core theme in Earth system science. *Aeolian Research*, *2*, 181–204. https://doi.org/10.1016/j.aeolia.2011.02.001

Sow, M., Alfaro, S. C., Rajot, J. L., & Marticorena, B. (2009). Size resolved dust emission fluxes measured in Niger during 3 dust storms of the AMMA experiment. *Atmospheric Chemistry and Physics*, *9*(12), 3881–3891. https://doi.org/10.5194/acp-9-3881-2009

Stegmann, P. G., & Yang, P. (2017). A regional, size-dependent, and causal effective medium model for Asian and Saharan mineral dust refractive index spectra. *Journal of Aerosol Science*, *114*, 327–341. https://doi.org/10.1016/J.JAEROSCI.2017.10.003

Tegen, I. (2003). Modeling the mineral dust aerosol cycle in the climate system. *Quaternary Science Reviews*, *22*, 1821–1834. https://doi.org/10.1016/S0277-3791(03)00163-X

Textor, C., Schulz, M., Guibert, S., Kinne, S., Balkanski, Y., Bauer, S., et al. (2006). Analysis and quantification of the diversities of aerosol life cycles within AeroCom. *Atmospheric Chemistry and Physics*, *6*, 1777–1813.

Vogel, B., Hoose, C., Vogel, H., & Kottmeier, C. (2006). A model of dust transport applied to the Dead Sea area. *Meteorologische Zeitschrift*, *15*(6), 611–624. https://doi.org/10.1127/0941-2948/2006/0168

Wagner, R., Ajtai, T., Kandler, K., Lieke, K., Linke, C., Mueller, M., et al. (2012). Complex refractive indices of Saharan dust samples at visible and near UV wavelengths: A laboratory study. *Atmospheric Chemistry and Physics*, *12*, 2491–2512. https://doi.org/10.5194/acp-12-2491-2012

Wiegner, M., Gasteiger, J., Kandler, K., Weinzierl, B., Rasp, K., Esselborn, M., et al. (2009). Numerical simulations of optical properties of Saharan dust aerosols with emphasis on lidar applications. *Tellus*, *61*, 180–194. https://doi.org/10.1111/j.1600-0889.2008.00381.x

Winker, D. M., Tackett, J. L., Getzewich, B. J., Liu, Z., Vaughan, M. A., & Rogers, R. R. (2013). The global 3-D distribution of tropospheric aerosols as characterized by CALIOP. *Atmospheric Chemistry and Physics*, *13*(6), 3345–3361. https://doi.org/10.5194/acp-13-3345-2013

Winker, D. M., Vaughan, M. A., Omar, A., Hu, Y., Powell, K. A., Liu, Z., et al. (2009). Overview of the CALIPSO mission and CALIOP data processing algorithms. *Journal of Atmospheric and Oceanic Technology*, *26*(11), 2310–2323. https://doi.org/10.1175/2009JTECHA1281.1

Yi, B., Hsu, C. N., Yang, P., & Tsay, S.-C. (2011). Radiative transfer simulation of dust-like aerosols: Uncertainties from particle shape and refractive index. *Journal of Aerosol Science*, *42*(10), 631–644. https://doi.org/10.1016/j.jaerosci.2011.06.008

Zängl, G., Reinert, D., Rípodas, P., & Baldauf, M. (2015). The ICON (icosahedral non-hydrostatic) modelling framework of DWD and MPI-M: Description of the non-hydrostatic dynamical core. *Quarterly Journal of the Royal Meteorological Society*, *141*(687), 563–579. https://doi.org/10.1002/qj.2378